

Monthly quasi-periodic eruptions from repeated stellar disruption by a massive black hole

Received: 23 February 2023

Accepted: 7 August 2023

Published online: 7 September 2023

 Check for updates

P. A. Evans¹✉, C. J. Nixon^{1,2}, S. Campana³, P. Charalampopoulos^{4,5},
D. A. Perley⁶, A. A. Breeveld⁷, K. L. Page¹, S. R. Oates⁸,
R. A. J. Eyles-Ferris¹, D. B. Malesani^{9,10,11}, L. Izzo^{11,12}, M. R. Goad¹,
P. T. O'Brien¹, J. P. Osborne¹ & B. Sbarufatti³

In recent years, searches of archival X-ray data have revealed galaxies exhibiting nuclear quasi-periodic eruptions with periods of several hours. These are reminiscent of the tidal disruption of a star by a supermassive black hole. The repeated, partial stripping of a white dwarf in an eccentric orbit around an $\sim 10^5 M_{\odot}$ black hole provides an attractive model. A separate class of periodic nuclear transients, with much longer timescales, have recently been discovered optically and may arise from the partial stripping of a main-sequence star by an $\sim 10^7 M_{\odot}$ black hole. No clear connection between these classes has been made. We present the discovery of an X-ray nuclear transient that shows quasi-periodic outbursts with a period of weeks. We discuss possible origins for the emission and propose that this system bridges the two existing classes outlined above. This discovery was made possible by the rapid identification, dissemination and follow-up of an X-ray transient found by the new live Swift-XRT transient detector, demonstrating the importance of low-latency, sensitive searches for X-ray transients.

Swift J023017.0+283603 (hereafter Swift J0230) was discovered in Swift X-ray Telescope (XRT) data by the Living Swift-XRT Point Source (LSXPS) catalogue's real-time transient detector¹ on 2022 June 22 (ref. 2). The source was serendipitously present in an observation of an unconnected source, SN 2021afk (4.3' away) and had a 0.3–10 keV count rate of $2.7^{+0.6}_{-0.5} \times 10^{-2}$ counts s^{-1} . This field had been observed on 11 previous occasions by Swift between December 2021 and January 2022. After combining all those observations, Swift J0230 was still undetected

down to a 3σ upper limit of 1.5×10^{-3} counts s^{-1} . The last of these observations was 164 days before the discovery of Swift J0230, placing a rather loose lower limit on its switch-on time. For convenience, we give all times relative to modified Julian date (MJD) 59752 (midnight on the day of the discovery). The best localization of Swift J0230 is from the XRT, being RA = 02 h 30 min 17.12 s, dec. = +28° 36' 04.4" (J2000), with an uncertainty of 2.8" (radius, 90% confidence). This is consistent with the nucleus of the galaxy 2MASX J02301709+2836050, but also

¹School of Physics and Astronomy, University of Leicester, Leicester, UK. ²School of Physics and Astronomy, University of Leeds, Leeds, UK. ³INAF, Osservatorio Astronomico di Brera, Merate, Italy. ⁴Department of Physics and Astronomy, Tuorla Observatory, Turku, Finland. ⁵DTU Space, Technical University of Denmark, Kongens Lyngby, Denmark. ⁶Astrophysics Research Institute, Liverpool John Moores University, Liverpool, UK. ⁷Mullard Space Science Laboratory, University College London, Dorking, UK. ⁸School of Physics and Astronomy & Institute for Gravitational Wave Astronomy, University of Birmingham, Birmingham, UK. ⁹Department of Astrophysics/IMAPP, Radboud University, Nijmegen, the Netherlands. ¹⁰Cosmic Dawn Center (DAWN), Copenhagen, Denmark. ¹¹Niels Bohr Institute, University of Copenhagen, Copenhagen, Denmark. ¹²INAF-Osservatorio Astronomico di Capodimonte, Naples, Italy. ✉e-mail: pae9@leicester.ac.uk

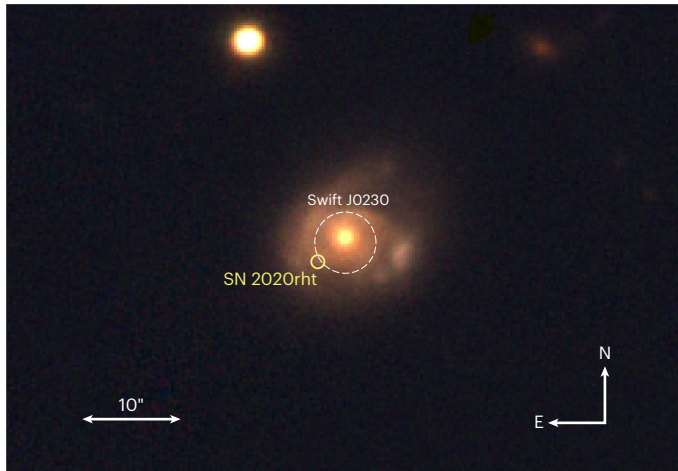


Fig. 1 | Location of the new transient, Swift J0230, relative to its host galaxy and an old supernova. The image is an archival Pan-STARRS⁴⁴ image of 2MASX J02301709+2836050, with colour scaled arbitrarily for aesthetic purposes. The broken circle shows the 90% confidence Swift-XRT position of Swift J0230, and the solid one SN 2020rht.

marginally consistent with the type-II supernova SN 2020rht (3.1" away), which had been discovered 2 years earlier on 2020 August 12 (ref. 3; Fig. 1). An optical spectrum of 2MASX J02301709+2836050, obtained with the Nordic Optical Telescope (NOT; Fig. 2), gives a redshift $z = 0.03657 \pm 0.00002$. Assuming standard cosmological parameters⁴, this corresponds to a luminosity distance $D_L = 160.7$ Mpc. The galaxy type is unclear, but it is either quiescent or, at most, a very weak active galactic nucleus (AGN; Supplementary Information).

Results

X-ray analysis

Following the initial, serendipitous discovery, we undertook regular monitoring with Swift (see Methods for details). The initial outburst continued for 4 d following the discovery. On the fourth day, it ended with a rapid decay, the luminosity falling by a factor of 20 in just 57 ks. There was a brief rebrightening (by a factor of 4.5 in 6 ks), before it became too faint to detect. The light curve is shown in Fig. 3. Fitting this decay of luminosity with a power law, $L \propto (t - t_0)^{-\alpha}$ (where t_0 is the start of the first bin in this observation), gives $\alpha = 11.0 \pm 1.7$. Eight subsequent outbursts were observed at ~ 25 d intervals, with durations of ~ 10 – 15 d. The fifth outburst was either substantially longer (up to ~ 32 d), or consisted of a weak outburst, a return to quiescence, and then a second, longer outburst. This was followed by a long gap of ~ 70 d during which two possible short and weak outbursts were seen, before another outburst like the early ones.

A Lomb–Scargle analysis (Methods and Extended Data Fig. 1) revealed moderately significant peaks at approximately 22 and 25 d periods, although each peak is ~ 1 d wide, confirming the quasi- rather than strictly periodic nature of the variability, as may be expected from eyeballing the light curve. Further consideration of the variability required us to define what constitutes an outburst. The initial outburst and that from days -41 – 48 appear clearly defined, but during the outburst from days -60 – 75 , the source underwent a sudden decline, being undetected on day 72 with an upper limit of $L < 8.9 \times 10^{41}$ erg s⁻¹ (0.3–2 keV), recovering to $L \approx 2 \times 10^{42}$ erg s⁻¹ by day 74. It seems plausible to interpret this as a single outburst with a sudden, brief dip. Hereafter, what constitutes an outburst becomes more subjective. The outbursts starting on days 89 and 102 could each be explained as comprising two short outbursts close together or a single outburst with a quiet phase in the middle. Note that in the first of these, if we sum the upper limits during this quiet phase, we find a detection at a higher level than the

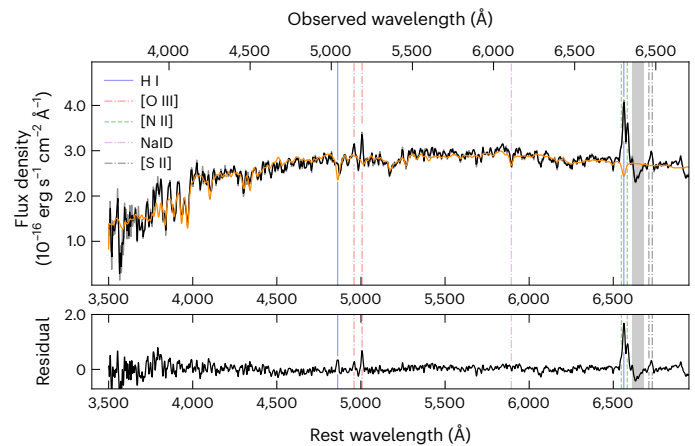


Fig. 2 | Optical spectrum of the host galaxy 2MASX J02301709+2836050 obtained with the NOT on day 132. Top, the black line shows the observed spectrum, while the orange line shows the fit to the stellar continuum provided by STARLIGHT. The vertical lines mark prominent emission and absorption features, which together allowed us to measure the redshift $z = 0.03657 \pm 0.00002$ (1σ confidence). Bottom, the residuals between the observed data (stellar + nebular spectrum) and the fit (stellar continuum), which single out the nebular emission. The emission-line fluxes were measured from the residual spectrum and allowed us to place the galaxy on a BPT plot (Extended Data Fig. 3).

upper limits found in the quiescent phases. During the long, largely quiescent period from days 111 to 195, the source was twice briefly detected with $L \approx 1$ – 2×10^{41} erg s⁻¹, but these are hardly ‘outbursts’ in the same way as the earlier emission. Based on visual inspection of the light curve, we defined an outburst as comprising any times where $L > 2 \times 10^{41}$ erg s⁻¹. Details of the outbursts thus identified are given in Table 1. See Methods for full details of how these were derived. In summary, we detected transient X-ray emission that rapidly switches on and off again with a recurrence timescale that is of the order of 25 d but which can vary by several days between outbursts. The duration of the outbursts also shows significant variability with the longest being of the order of 20 d and the shortest less than a day.

The X-ray spectrum during the outbursts was very soft, with no emission seen above 2 keV, and could be modelled well with a simple black-body emitter with only Galactic absorption. Due to this soft spectrum, the typical energy bands used for XRT hardness ratios were inappropriate. We selected 0.3–0.9 keV and 0.9–2 keV as this gave roughly equal counts in the two bands, thus maximizing the signal-to-noise ratio. The time evolution of this hardness ratio (Fig. 3) shows a clear correlation between luminosity and spectral hardness (Spearman rank P value of 1.3×10^{-6} for the data being uncorrelated), ruling out a change in absorption as the cause of the flux variation. We fitted the absorbed black-body model to each observation in which Swift J0230 was detected. The black-body temperature obtained is strongly correlated with luminosity (P value, 4.5×10^{-6} ; Extended Data Fig. 2). No evidence for absorption beyond the Galactic column was seen.

As noted earlier, although coincident with a galaxy nucleus, the XRT position is also potentially in agreement with that of SN 2020rht. We obtained a 3 ks Chandra director’s discretionary time observation during the fourth outburst to obtain a better position, but unfortunately, this observation fell on day 97, which turned out to be in one of the mid-outburst quiet phases.

Optical and ultraviolet analysis

At optical and ultraviolet wavelengths, there is no evidence for outbursting behaviour. We obtained data from both the Swift Ultraviolet/Optical Telescope (UVOT) and the Liverpool Telescope (LT; Extended Data Tables 1 and 2). The host galaxy, 2MASX J02301709+2836050, is

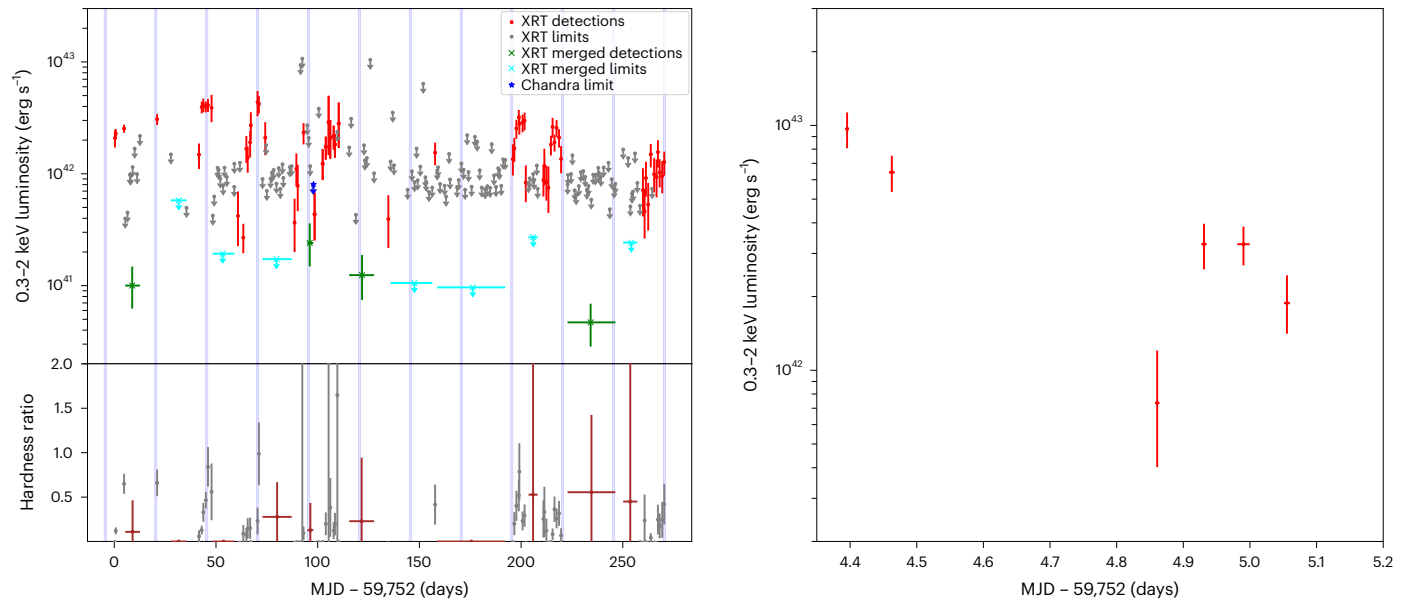


Fig. 3 | The temporal evolution of Swift J0230. All error bars are 1σ significance. Left, X-ray time series, binned to one bin per observation. Top, 0.3–2 keV luminosity light curve. The red data points marked with dots are the Swift-XRT detections. Grey arrows are 3σ upper limits from XRT. The dark blue upper limit marked with an asterisk is from Chandra. The broad bins marked with crosses were created by combining consecutive XRT non-detections (upper limits in cyan

and detections in green). See Methods for full details. Bottom, the (0.9–2)/(0.3–0.9) keV hardness ratio. The spectral hardness is strongly correlated with the luminosity. The vertical bands are at 25 d intervals. Right, light curve of the XRT observations taken on days 4 and 5, with one bin per spacecraft orbit, showing the rapid decay at the end of the first outburst. All error bars are at the 1σ level.

Table 1 | Constraints on the timescales of the observed outbursts

Outburst	Start		End		Duration		Period	
	MJD min	MJD max	MJD min	MJD max	min (d)	max(d)	min (d)	max(d)
1	59,587.9	59,752.3	59,757.3	59,757.4	4.9	169.5		
2	59,763.2	59,773.0	59,773.1	59,787.5	0.1	24.3	10.9	185.1
3	59,787.5	59,793.7	59,799.8	59,800.4	6.2	12.9	14.5	30.4
4	59,811.0	59,815.3	59,826.4	59,827.0	11.1	16.0	17.3	27.8
5	59,839.2	59,841.5	59,862.3	59,867.5	20.8	28.3	24.0	30.5
6	59,870.8	59,886.7	59,886.7	59,887.9	0.0	17.0	29.3	47.5
7	59,908.3	59,909.7	59,909.7	59,910.8	0.0	2.4	21.6	38.9
8	59,942.3	59,948.0	59,954.3	59,955.6	6.4	13.4	32.5	39.6
9	59,960.2	59,963.0	59,971.7	59,974.8	8.7	14.7	12.2	20.7
10	60,010.8	60,011.9	60,022.4 ^a	–	11.6 ^a	–	47.8	51.8

^aThe final outburst was ongoing when observations ended.

clearly detected in all observations, but there is no evidence for variability or an increase in flux compared to catalogued values. We also analysed UVOT data from the pre-discovery observations and found no secure evidence for a change in brightness between those data and the observations taken during the outburst. Full details are given in Methods.

Discussion

The peak luminosity of $\sim 4 \times 10^{42} \text{ erg s}^{-1}$, the timescales of the outbursts and their quasi-periodic, quasi-chaotic nature, the soft X-ray spectrum and the lack of optical variability place strong constraints on possible models that explain Swift J0230. Although the lack of detection with Chandra means that we cannot rule out a positional association with SN 2020rht, it is difficult to see how a supernova could have evolved into the object that we have detected. The spectrum, luminosity and variability timescale are inconsistent with the properties of ultra-luminous

X-ray sources⁵. Although certain supernovae could in principle be followed by X-rays from a newly formed millisecond pulsar⁶, this should occur while the supernova is still visible in the optical. Margalit et al.⁷ showed how this emission could be delayed, but the timescales and luminosities they predict (for example, their Fig. 5) are not consistent with our observation. Equally, neither model explains the variability or spectrum we see in Swift J0230. We discuss this further in the Supplementary Information.

We suggest that (near) periodic mass supply into an accretion flow onto the central supermassive black hole in 2MASX J02301709+2836050 is the most likely explanation for Swift J0230. From simple energetics (Supplementary Information), we can infer that the total mass accreted during a typical outburst is $\sim 10^{-5} M_{\odot}$. In an AGN, flares and outbursts are common from a supermassive black hole at the heart of the galaxy accreting from a surrounding disc of gas. However, the timescale and spectrum of Swift J0230 are not consistent

with typical AGN behaviour, and 2MASX J02301709+2836050 itself does not appear to be an AGN (Extended Data Fig. 3; see Supplementary Information for a full discussion). We, therefore, consider the possibility that one (or several) stars are interacting with, and feeding mass onto, the central supermassive black hole. One possible mechanism for producing the mass flow is the interaction of two stars in orbit around the black hole. If they pass sufficiently close to each other, material can be liberated from one or both stars that can feed the central black hole^{8,9}. To generate the required timescales from this model requires a pair of stars orbiting in the same direction and in the same plane⁹. This could occur for stellar orbits that are initially randomly oriented, if they can be subsequently ground down into the same plane by interaction with an AGN disc¹⁰. For Swift J0230, which lacks any clear signature of a standard AGN disc, it is unlikely that any stars orbiting the central black hole have the required orbits to achieve the observed timescales.

Another possibility is a repeating, partial tidal disruption event (rpTDE), in which a star on a bound, highly eccentric orbit loses some of its envelope every pericentre passage due to tides from the black hole's gravitational field. These events are a subclass of TDEs in which the 'regular' scenario sees the incoming star approach the black hole on a parabolic orbit and the star is destroyed by the first encounter (see refs. 11,12 for reviews of TDEs).

The rpTDE model was investigated before the discovery of any corresponding sources (for example, ref. 13) and was suggested as the explanation of X-ray flares in the active galaxy IC 3599 (ref. 14). Recently, it has been proposed (for example, refs. 15–17) as a possible explanation for hours-long quasi-periodic eruptions (QPEs) discovered in galactic nuclei (for example, refs. 18–22). These works focused on the possibility of a white dwarf interacting with a relatively low-mass central black hole of mass $\sim 10^{5-6} M_{\odot}$. A second set of sources show much longer outbursts (both in duration and recurrence period) and have been referred to as periodic nuclear transients (PNTs). These may be the same rpTDE mechanism acting with a main-sequence star, rather than a compact star^{23–26}, and a more massive black hole ($\sim 10^{7-8} M_{\odot}$).

In the rpTDE model, the donor star is in a highly eccentric orbit around a black hole. At each pericentre passage, the star has to approach, but not quite reach, the tidal radius at which the star would be fully disrupted. The outer layers of the star are liberated, and some of this material accretes onto the central black hole to power the outburst. The recurrence time of the outbursts is related to the orbital period of the star. The majority of the energy released from the accretion process occurs in the central regions near the black hole where the matter is most likely in the form of an accretion disc. We can, therefore, provide an estimate of the black hole mass in Swift J0230 by comparing the temperature of ~ 100 eV ($\sim 10^6$ K), measured from the X-ray spectrum, with the peak temperature of a standard accretion disc²⁷. This yields a mass estimate for the black hole of $\sim 2 \times 10^5 M_{\odot}$ (Supplementary Information). This is close to the mass estimates for QPE sources (for example, refs. 18,19,22). Note that QPE sources and Swift J0230 show very little in the way of optical emission, whereas the PNTs show strong optical emission. This may simply reflect the difference in the black hole masses. That is, the soft X-ray spectrum and the lack of optical emission seen for Swift J0230 appear consistent with this estimate of the black hole mass.

If the accreted material is stripped from the orbiting star during the pericentre passage of a highly elliptical orbit and the pericentre distance is a few gravitational radii (required to liberate any material from the surface of a white dwarf for black hole masses of a few $10^5 M_{\odot}$), then we would expect the outburst duration to be similar in different systems, regardless of their orbital (and hence outburst) period. This is because the pericentre passage of a highly elliptical orbit is approximately that of a parabolic orbit and its duration is not connected to the orbital period. This means that it is difficult to explain both Swift J0230 (outburst duration of days) and the pre-existing QPEs (outburst duration of hours) as an rpTDE of a white dwarf around a modest-mass black hole. On the other hand, an rpTDE of a main-sequence star by

an $\sim 10^7\text{--}10^8 M_{\odot}$ black hole has been proposed to explain the PNTs ASASSN-14ko, for which the recurrence timescale is 114 d (refs. 23,24), and AT2018fyk, which exhibited a significant rebrightening after around 600 d of quiescence²⁵. Swift J0230 clearly lies between these two classes of object.

An important question is how the star arrived on such an orbit around the central black hole. Tidal capture, in which an orbiting star loses orbital energy due to tidal forces and becomes bound to the black hole²⁸, is typically incapable of generating the required orbits; however, the Hills mechanism²⁹ has been proposed as a viable formation route for the PNT ASASSN-14ko (ref. 30). In this mechanism, a binary star system approaches the black hole with a small enough pericentre distance such that the tidal force from the black hole is stronger than the gravitational force holding the binary together. This results in the binary being disrupted, with one component being ejected from the system and the other becoming locked into a bound, but highly eccentric, orbit about the black hole. If the progenitor of Swift J0230 were a binary consisting of a low-mass, main-sequence star and, say, a white dwarf, then the main-sequence star needs to be captured into a bound orbit around the black hole with the observed ~ 25 d period. For a black hole mass of $M_{\bullet} \approx 4 \times 10^5 M_{\odot}$, this period corresponds to the most likely outcome of Hills capture from such a binary system (the calculations of³⁰ show that higher black hole masses are allowed but are significantly less likely to result in this period for the bound star; see Supplementary Information for details). This is consistent with the mass estimate derived from the temperature of the X-ray spectrum. Further, the expected accretion timescales from such a system (Supplementary Information) are also consistent with those observed in Swift J0230.

The variable shape and timescales of the outbursts seen in Swift J0230 may also be explained by this model. In a standard TDE, as opposed to an rpTDE, the star arrives on a parabolic orbit, meaning that some of the stellar matter is bound to the black hole (the inner tidal stream), and this material forms an accretion flow, whereas the rest of the stellar debris (the outer tidal stream) is unbound and leaves the system¹¹. In an rpTDE, the star must be on a bound orbit around the black hole. In this case, both the inner and outer tidal streams can remain bound to the black hole. The inner stream falls back soonest and, thus, has a higher mass return rate, whereas the outer stream can return on longer timescales. Due to relativistic precession of the stellar debris orbits (both apsidal and nodal), the returning streams can collide and partially cancel their angular momenta to augment the accretion rate onto the black hole, with the magnitude of the effect depending on the orientation of the colliding orbits (see refs. 31,32 for similar variability induced in accretion discs due to relativistic precession; the processes described therein may also occur in the discs formed in Swift J0230). The exact details of this interaction between the two streams, the accretion flow and the orbiting star are complex and require a full numerical analysis, which is beyond the scope of this discovery paper; however it is clear that such an interaction will produce variable emission that could at least partially erase the more exactly periodic nature of the stellar orbit. An example of such complex interacting debris streams can be seen in Fig. 9 of ref. 33. It will be particularly important to determine if the star itself can be sufficiently perturbed during each pericentre passage, with, for example, tides imparting variations in oscillation amplitudes and rotation frequency and, thus, change the amount of mass transferred and the structure of each outburst. Additionally, the sharp decline observed at the end of each outburst may be driven by the returning star disturbing the accretion flow. These questions can be addressed with future theoretical investigations.

We have proposed a single explanation for the QPEs and PNTs, as a repeated, partial, tidal disruption of a star in an eccentric orbit around a supermassive black hole. We have reported the discovery of an object that can bridge the gap between these classes. The QPEs are thought to be due to a white dwarf and a modest black hole ($\sim 10^5 M_{\odot}$), whereas the PNTs are thought to occur for a main-sequence star and

a more massive black hole ($\sim 10^7 M_\odot$). Swift J0230 represents an intermediate class of system, which is consistent with a main-sequence star orbiting a modest-mass black hole. Given the timescales, modest fluxes and lack of emission outside of the X-ray band, Swift J0230-like systems are difficult to discover. Unlike QPEs, which can be discovered in archival data, their timescales and behaviour are not exposed by a single observation. It is only with the recent creation of a real-time transient detector¹ that objects like this can be found rapidly enough for follow-up observations to expose their behaviour. That this event was found within 3 months of enabling this real-time search suggests that they are reasonably common, and we can expect to discover more objects of this class with sensitive, wide-field X-ray instruments such as eRosita³⁴ and in the near future, the Einstein Probe³⁵.

Methods

Discovery

At 13.58 UTC on 2022 June 22, the LSXPS real-time transient detector¹ reported the discovery of a possible new X-ray transient, dubbed Swift J023017.0+283603. The object was detected in Swift observation 00014936012, which had taken place between 08.19 and 08.46 UTC; that is the notification was produced 5.2 h after the observation. (Most of this latency related to the timing of ground station passes and the ingesting of the data by the Swift Data Center. The observation data were received at the UK Solar System Data Centre at 13.51 UTC.) No catalogued X-ray source was found at this position. Further, Swift had already observed this location on 11 previous occasions (the observation target was SN 2021afkk, 4.3' away from this serendipitous transient), for a total of 9.6 ks. These observations had been analysed as a stacked image in LSXPS (Dataset ID 19690); no source was present near the position of Swift J0230, with a 3σ upper limit of 1.5×10^{-3} counts s^{-1} . The peak count rate of Swift J0230 in the new observation was $2.7_{-0.5}^{+0.6} \times 10^{-2}$ counts s^{-1} (1σ errors), significantly above this upper limit, clearly indicating that a new transient had been discovered.

Due to the very soft spectrum and coincidence with the nucleus of the galaxy 2MASX J02301709+2836050, this was originally interpreted as a TDE^{2,36}, and a high-urgency target-of-opportunity request was submitted to Swift.

In the following analysis, we assume that $H_0 = 67.36$ km s^{-1} Mpc⁻¹, $\Omega_\Lambda = 0.6847$ and $\Omega_m = 0.3153$ (ref. 4).

Observations and data analysis

Swift follow-up observations began at 16.07 UTC on June 22 (TO + 0.67 d). Due to Swift's Moon observing constraint, subsequent observations were not available until day 4 (June 26). Daily observations of 1 ks exposure were obtained with Swift until day 12. A subsequent target-of-opportunity request was submitted (Principal Investigator, Guolo) for weekly monitoring of this source, which began on day 21 (2022 July 13). The initial observation showed that the source had resumed emitting X-rays, but in the following observations on days 27 and 35, it was again below the detection threshold. To better quantify the duty cycle, we submitted regular target-of-opportunity requests (Principal Investigator, Evans) for daily 1 ks observations, which ran until 2023 March 19 (day 270) when the source entered Swift's Sun observing constraint. Note that we did not obtain 1 ks per day, as each month proximity to the Moon prevented observations for 3–4 days. Moreover, due to the nature of Swift's observing programme, our observations were sometimes shortened or completely superseded by other targets.

Swift-XRT. XRT data were analysed using the on-demand tools of ref. 37, via the swifttools Python module (v.3.0.7). A 0.3–10 keV light curve was constructed, binned to one bin per observation; the soft and hard bands were set to 0.3–0.9 and 0.91–2 keV respectively. Observations 00015231018 and 00015231019 overlapped in time, as did 0001523143 and 0001523144. When this happens, the per-observation

binning is unreliable, so we built light curves for each of these observations individually, and then replaced the affected bins in the original light curves with those thus obtained. For each run of consecutive upper limit bins, we merged the limits into a single bin, using the MergeLightCurveBins() function in swifttools, giving a better measurement of, or limit on, the quiescent flux.

For each observation in which the light curve showed a detection (at the 3σ level), we extracted a spectrum, fitting it with a black-body component absorbed by two absorbers. The first was a tbabs model with N_H fixed at the Galactic value of 1.12×10^{21} cm⁻² (ref. 38). The second was a ztbabs model with N_H free to vary and the redshift fixed at the value obtained from our NOT spectrum. From these fits, we obtained the 0.3–2 keV flux and (given the luminosity distance of 160.7 Mpc) the luminosity. The dependence of this luminosity on the black-body temperature, as reported in the main paper, is shown in Extended Data Fig. 2. We also obtained for each spectrum the conversion factor from the 0.3–10 keV count rate to the 0.3–2 keV luminosity, and so converted our count-rate light curve into luminosity. For the detections with too few photons to yield a spectral fit, the upper limits in the light curve and the bins created by merging (above), we used the conversion factor of 7.54×10^{43} erg per count obtained from the discovery observation. The resultant light curve is shown in Fig. 3, with the merged bins marked with crosses (and in green/cyan in the online version). To explore the rapid flux decay seen at the end of the first outburst (right-hand panel of Fig. 3), we rebinned the data to one bin per snapshot (using the rebinLightCurve() function), converting to luminosity using the same conversion factor (that obtained for the appropriate observation) for each bin.

To determine the timescales of the outbursts (Table 1), we defined outbursts as being times when the 0.3–2 keV luminosity was above 3×10^{41} erg s^{-1} (based on visual inspection of the light curve). We built a new light curve, still with one bin per observation, but in which all bins were created as count rates with 1σ errors, rather than allowing upper limits (using the swifttools module with the argument allowUL=False passed to the light curve), and then identified each point that was inconsistent with $L = 3 \times 10^{41}$ erg s^{-1} at at least the 1σ level. The start and end times of the outbursts were then constrained to being between consecutive data points from this sample that were on opposite sides of the 3×10^{41} erg s^{-1} line. The results are shown in Table 1. We created a Lomb–Scargle periodogram (using the astropy.timeseries.LombScargle Python package) to search this light curve for periodicity. We found possible peaks centred on 22.1 and 25.0 d, each with widths of ~ 1 d. To determine their significance, we used a bootstrapping method in which we 'shuffled' the data, randomly redistributing the fluxes (and their errors) among the time bins, and then recalculated the periodogram. We did this 10,000 times. For each trial period in the periodogram, we identified the 99.7th percentile of power, that is the 3σ significance threshold. The result is shown in Extended Data Fig. 1, along with the window function. These two peaks are both clearly above 3σ in significance and not present in the window function.

We also investigated whether we could rule out short-period variations with our observing strategy, like those seen in the QPEs reported to date. We simulated a simplistic light curve based on the period of GSN 069 (and including alternating between slightly longer and shorter cycles as in GSN 069). For each snapshot in the real XRT light curve of Swift J0230, we determined the phase of the trial period and set the count rate either to 0.03 counts s^{-1} (on) or 0.001 counts s^{-1} (off); fractional errors were set to typical values from our real light curve. We then constructed the Lomb–Scargle periodogram for this and repeated the bootstrap approach above. A strong signal was found at the nominal period, confirming that such a signal would have been easily recovered had it been present. Thus, we can be confident that there was no short-period modulation like that in GSN 069 present in Swift J0230.

Swift-UVOT. UVOT data were analysed using the `uvotsource` package in `heasoft` v.6.30. For the pre-outburst data, the location of Swift J0230 was only in the field of view on five occasions. No sign of variability was found in these data, so we summed the images in each filter using `uvotsum` and extracted mean magnitudes. In the initial discovery observation, UVOT gathered data in all filters, but no sign of the outburst was seen, any variability being swamped by the underlying galaxy emission. UVOT magnitudes from this observation and the pre-discovery data are shown in Extended Data Table 1. Due to this lack of variability, subsequent Swift observations used the UVOT ‘filter of the day’, which rotates each day between the *u* and ultraviolet filters, to preserve the life of the filter wheel. No significant variability was seen. When visually examining the light curve, it is tempting to claim some variability in phase with the XRT data, but the magnitude of the variability is much smaller than the errors on the UVOT photometry. To further investigate, we rebinned the XRT light curve to one bin per snapshot (that is the same binning as the UVOT data, which has one exposure per snapshot) and disabled upper limits, forcing a count rate and 1σ error per bin. For each UVOT filter, we identified the coincident XRT data and then performed a Spearman rank correlation analysis between the XRT and UVOT fluxes. This did not account for the uncertainty on the count rates, and therefore was likely to overestimate the significance; however, no significant correlation was found at all, with *P* values between 0.1 and 0.9, and so more complex correlation mechanisms were not deemed necessary. We also attempted image subtraction, summing all UVOT images in the *u* filter (which showed the strongest signs of possible variability) during times of XRT detection and non-detection, before subtracting the latter from the former. No evidence of an excess at the XRT position was seen.

Nordic Optical Telescope. Spectroscopy of the host galaxy 2MASX J02301709+2836050 was obtained on 2022 November 1 (day 132). A 2.4 ks optical spectrum was accumulated using the Alhambra Faint Object Spectrograph and Camera mounted on the 2.56 m NOT located at La Palma, Spain. The spectrum was reduced using the spectroscopic data reduction pipeline PyNOT (<https://github.com/jkrogager/PyNOT>). We used a 1.0 inch slit width and grism no. 4, covering the wavelength range $\sim 3,200\text{--}9,600\text{ \AA}$ at resolution $\Delta\lambda/\lambda \approx 360$. The airmass during the observation was of the order of ~ 1.1 . The spectrum is shown in Fig. 2, and features prominent H α , [N II] and [O III] emission lines, with a common redshift of 0.03657 ± 0.00002 . A weak H β line is also seen. The flux of weaker lines is often affected by the presence of stellar absorption in the continuum. To recover the pure nebular fluxes, we fitted the spectrum with the STARLIGHT software (<http://www.starlight.ufsc.br/>). STARLIGHT fits the stellar continuum, identifying the underlying stellar populations in terms of age and metallicity. By comparing the observed data with the output synthetic spectrum, the pure nebular continuum can be identified and the emission-line fluxes measured accurately.

Based on this analysis, we could build the Baldwin, Phillips and Terlevich (BPT) diagram³⁹. Such diagrams are widely adopted to identify the level of nuclear activity in a galaxy. It exploits the ratio of nearby emission lines, minimizing the effects of extinction. The result is shown in Extended Data Fig. 3. 2MASX J02301709+2836050 lies in the locus where a low-power AGN, a low-ionization nuclear emission-line region and star-forming dominated galaxies intersect. A secure classification of 2MASX J02301709+2836050 is, therefore, not possible, but a powerful AGN is clearly ruled out.

Liverpool Telescope. The position of Swift J0230 was observed with the optical imager (IO:O) of the 2 m LT on six different occasions between 2022 Jun 28 and 2022 Aug 26, using the griz filters (the first and last epoch were gri only). Images were processed using the default IO:O pipeline and downloaded from the LT archive. We co-added exposures and performed basic image subtraction versus Pan-STARRS1

reference imaging using a custom IDL (Interactive Data Language) routine. Although a few subtracted image pairs show weak positive or negative residuals at the location of the ~ 18 mag nuclear point source, there is no clear correlation in these residuals between filters or epochs, suggesting minimal contribution of any nuclear transient (or any AGN variability) to the optical flux at the sensitivity level of the LT images. The lack of any residual source at the location of SN 2020rht is unambiguous in all images. Limiting magnitudes of the images (5σ) are given in Extended Data Table 2.

Chandra. We requested a 3 ks director’s discretionary time observation of Swift J0230 with Chandra (Proposal 23708869). We triggered this on day 93, when the Swift-XRT count rate exceeded the approved threshold of $0.02\text{ counts s}^{-1}$, and the observations were obtained on day 97 (observation ID 27470). Our intention was to obtain an accurate (arc-second or better) position of Swift J0230, to be able to say definitively whether it was associated with the nucleus of its host, the historical supernova or neither. Unfortunately, this observation occurred during the quiescent/faint part of the fifth outburst, and Swift J0230 was not detected. The 3σ upper limit, converted to $0.3\text{--}2\text{ keV}$ luminosity assuming a 90 eV black body with a Galactic absorber, is $L < 8.0 \times 10^{41}\text{ erg s}^{-1}$, consistent with the XRT measurements at the time (Fig. 3).

Data availability

All the Swift data are available via the Swift data archives provided in the USA (<https://swift.gsfc.nasa.gov/archive/>), UK (<https://www.swift.ac.uk/archive/>) and Italy (<https://www.ssd.cnr.it/mmia/index.php?mission=swiftmastr>). The target IDs are 00014936 and 00015231. Reduced Swift-XRT data for this transient are available at <https://www.swift.ac.uk/LXSPS/transients/690>. The Chandra data are publicly available via the Chandra data archive (<https://cxc.harvard.edu/cda/>), with sequence 704871 and observation ID 27470. The NOT data will be available through the NOT public interface after the expiration of the standard proprietary period. The reduced spectrum is available through the University of Leicester FigShare repository (<https://doi.org/10.25392/leicester.data.c.6444296>). The LT data will be available through the LT public interface after the expiration of the standard proprietary period. The photometry was included in this published article.

Code availability

The IDL code used for the Liverpool Telescope data analysis is available from D. Perley on request.

References

1. Evans, P. A. et al. A real-time transient detector and the living Swift-XRT point source catalogue. *Mon. Not. R. Astron. Soc.* **518**, 174–184 (2023).
2. Evans, P. A., Campana, S. & Page, K. L. Swift J023017.0+283603: a possible tidal disruption event. *Astron. Telegr.* **15454**, 1 (2022).
3. Tonry, J. et al. ATLAS transient discovery report for 2020-08-13. *Transient Name Server Discovery Report* **2020-2472**, 1 (2020).
4. Planck Collaboration. et al. Planck 2018 results. VI. Cosmological parameters. *Astron. Astrophys.* **641**, A6 (2020).
5. Kaaret, P., Feng, H. & Roberts, T. P. Ultraluminous X-ray sources. *Annu. Rev. Astron. Astrophys.* **55**, 303–341 (2017).
6. Metzger, B. D., Vurm, I., Hascoët, R. & Beloborodov, A. M. Ionization break-out from millisecond pulsar wind nebulae: an X-ray probe of the origin of superluminous supernovae. *Mon. Not. R. Astron. Soc.* **437**, 703–720 (2014).
7. Margalit, B. et al. Unveiling the engines of fast radio bursts, superluminous supernovae, and gamma-ray bursts. *Mon. Not. R. Astron. Soc.* **481**, 2407–2426 (2018).
8. Metzger, B. D. & Stone, N. C. Periodic accretion-powered flares from colliding EMRIs as TDE imposters. *Astrophys. J.* **844**, 75 (2017).

9. Metzger, B. D., Stone, N. C. & Gilbaum, S. Interacting stellar EMRIs as sources of quasi-periodic eruptions in galactic nuclei. *Astrophys. J.* **926**, 101 (2022).
10. Syer, D., Clarke, C. J. & Rees, M. J. Star-disc interactions near a massive black hole. *Mon. Not. R. Astron. Soc.* **250**, 505–512 (1991).
11. Rees, M. J. Tidal disruption of stars by black holes of 10^6 – 10^8 solar masses in nearby galaxies. *Nature* **333**, 523–528 (1988).
12. Gezari, S. Tidal disruption events. *Annu. Rev. Astron. Astrophys.* **59**, 21–58 (2021).
13. Zalamea, I., Menou, K. & Beloborodov, A. M. White dwarfs stripped by massive black holes: sources of coincident gravitational and electromagnetic radiation. *Mon. Not. R. Astron. Soc.* **409**, L25–L29 (2010).
14. Campana, S. et al. Multiple tidal disruption flares in the active galaxy IC 3599. *Astron. Astrophys.* **581**, A17 (2015).
15. King, A. GSN 069 – a tidal disruption near miss. *Mon. Not. R. Astron. Soc.* **493**, L120–L123 (2020).
16. King, A. Quasi-periodic eruptions from galaxy nuclei. *Mon. Not. R. Astron. Soc.* **515**, 4344–4349 (2022).
17. Lu, W. & Quataert, E. Quasi-periodic eruptions from mildly eccentric unstable mass transfer in galactic nuclei. *Mon. Not. R. Astron. Soc.* <https://doi.org/10.1093/mnras/stad2203> (2023).
18. Miniutti, G. et al. Nine-hour X-ray quasi-periodic eruptions from a low-mass black hole galactic nucleus. *Nature* **573**, 381–384 (2019).
19. Giustini, M., Miniutti, G. & Saxton, R. D. X-ray quasi-periodic eruptions from the galactic nucleus of RX J1301.9+2747. *Astron. Astrophys.* **636**, L2 (2020).
20. Song, J. R. et al. Possible ~0.4 h X-ray quasi-periodicity from an ultrasoft active galactic nucleus. *Astron. Astrophys.* **644**, L9 (2020).
21. Chakraborty, J. et al. Possible X-ray quasi-periodic eruptions in a tidal disruption event candidate. *Astrophys. J. Lett.* **921**, L40 (2021).
22. Arcodia, R. et al. X-ray quasi-periodic eruptions from two previously quiescent galaxies. *Nature* **592**, 704–707 (2021).
23. Payne, A. V. et al. ASASSN-14ko is a periodic nuclear transient in ESO 253-G003. *Astrophys. J.* **910**, 125 (2021).
24. Payne, A. V. et al. The rapid X-ray and UV evolution of ASASSN-14ko. *Astrophys. J.* **926**, 142 (2022).
25. Wevers, T. et al. Live to die another day: the rebrightening of AT 2018fyk as a repeating partial tidal disruption event. *Astrophys. J. Lett.* **942**, L33 (2023).
26. Liu, Z. et al. Deciphering the extreme X-ray variability of the nuclear transient eRASSt J045650.3–203750. A likely repeating partial tidal disruption event. *Astron. Astrophys.* **669**, A75 (2023).
27. Shakura, N. I. & Sunyaev, R. A. Black holes in binary systems. Observational appearance. *Astron. Astrophys.* **24**, 337–355 (1973).
28. Fabian, A. C., Pringle, J. E. & Rees, M. J. Tidal capture formation of binary systems and X-ray sources in globular clusters. *Mon. Not. R. Astron. Soc.* **172**, 15 (1975).
29. Hills, J. G. Hyper-velocity and tidal stars from binaries disrupted by a massive galactic black hole. *Nature* **331**, 687–689 (1988).
30. Cufari, M., Coughlin, E. R. & Nixon, C. J. Using the Hills mechanism to generate repeating partial tidal disruption events and ASASSN-14ko. *Astrophys. J. Lett.* **929**, L20 (2022).
31. Nixon, C., King, A., Price, D. & Frank, J. Tearing up the disk: how black holes accrete. *Astrophys. J. Lett.* **757**, L24 (2012).
32. Raj, A. & Nixon, C. J. Disk tearing: implications for black hole accretion and AGN variability. *Astrophys. J.* **909**, 82 (2021).
33. Coughlin, E. R., Armitage, P. J., Nixon, C. & Begelman, M. C. Tidal disruption events from supermassive black hole binaries. *Mon. Not. R. Astron. Soc.* **465**, 3840–3864 (2017).
34. Predehl, P. et al. The eROSITA X-ray telescope on SRG. *Astron. Astrophys.* **647**, A1 (2021).
35. Yuan, W., Zhang, C., Chen, Y. & Ling, Z. in *Handbook of X-ray and Gamma-ray Astrophysics* (eds Bambi, C. & Santangelo, A.) 1–30 (Springer Singapore 2022).
36. Evans, P. A., Breeveld, A. A. & Oates, S. R. Further Swift observations of the TDE candidate Swift J023017.0+283603. *Astron. Telegr.* **15461**, 1 (2022).
37. Evans, P. A. et al. Methods and results of an automatic analysis of a complete sample of Swift-XRT observations of GRBs. *Mon. Not. R. Astron. Soc.* **397**, 1177–1201 (2009).
38. Willingale, R., Starling, R. L. C., Beardmore, A. P., Tanvir, N. R. & O’Brien, P. T. Calibration of X-ray absorption in our Galaxy. *Mon. Not. R. Astron. Soc.* **431**, 394–404 (2013).
39. Baldwin, J. A., Phillips, M. M. & Terlevich, R. Classification parameters for the emission-line spectra of extragalactic objects. *Publ. Astron. Soc. Pac.* **93**, 5–19 (1981).
40. Chambers, K. C. et al. The Pan-STARRS1 surveys. Preprint at <https://arxiv.org/abs/1612.05560> (2016).
40. Kewley, L. J., Dopita, M. A., Sutherland, R. S., Heisler, C. A. & Trevena, J. Theoretical modeling of starburst galaxies. *Astrophys. J.* **556**, 121–140 (2001).
41. Kauffmann, G. et al. Stellar masses and star formation histories for 10^5 galaxies from the Sloan Digital Sky Survey. *Mon. Not. R. Astron. Soc.* **341**, 33–53 (2003).
42. Schawinski, K. et al. Observational evidence for AGN feedback in early-type galaxies. *Mon. Not. R. Astron. Soc.* **382**, 1415–1431 (2007).
43. Tremonti, C. A. et al. The origin of the mass–metallicity relation: insights from 53,000 star-forming galaxies in the Sloan Digital Sky Survey. *Astrophys. J.* **613**, 898–913 (2004).

Acknowledgements

This work made use of data supplied by the UK Swift Science Data Centre at the University of Leicester. We acknowledge the following funding support: UK Space Agency (grant no. ST/X001881/1 to P.A.E., K.L.P., R.A.J.E.-F. and A.A.B.), the Science and Technology Facilities Council (grant no. ST/Y000544/1 to C.J.N. and grant no. ST/W000857/1 to P.T.O.B.), the Leverhulme Trust (grant no. RPG-2021-380 to C.J.N.), the Italian Space Agency (Contract ASI/INAF n. I/004/11/5 to S.C.), the European Union’s Horizon 2020 Programme under the AHEAD2020 project (grant no. 871158 to R.A.J.E.-F.) and the European Research Council under the European Union’s Horizon 2020 research and innovation programme (grant no. 725246 to D.B.M.). The Cosmic Dawn Center (DAWN) is funded by the Danish National Research Foundation under grant no. 140. The Pan-STARRS1 surveys and their public science archive have been made possible through contributions by the Institute for Astronomy, the University of Hawaii, the Pan-STARRS Project Office, the Max Planck Society and its participating institutes (the Max Planck Institute for Astronomy, Heidelberg, and the Max Planck Institute for Extraterrestrial Physics, Garching), Johns Hopkins University, Durham University, the University of Edinburgh, Queen’s University Belfast, the Harvard-Smithsonian Center for Astrophysics, Las Cumbres Observatory Global Telescope Network Incorporated, the National Central University of Taiwan, the Space Telescope Science Institute, the National Aeronautics and Space Administration under grant no. NNX08AR22G issued through the Planetary Science Division of the NASA Science Mission Directorate, the National Science Foundation (grant no. AST-1238877), the University of Maryland, Eotvos Lorand University, Los Alamos National Laboratory, and the Gordon and Betty Moore Foundation. L.I. was supported by grants from Villum Foundation (project nos. 16599 and 25501). We thank A. Beardmore for help with the bootstrapping method for the period analysis.

Author contributions

P.A.E. authored the tools that discovered the event, was the principal investigator of the Swift and Chandra observations, performed most of the X-ray data analysis and led the writing of the article. C.J.N. carried out the theoretical interpretation of the data and produced the associated text. S.C. first noticed the automated report of the new transient and classified it as of interest. He was Col of the Chandra observations. P.C. obtained the NOT spectrum and led the analysis of it, producing Fig. 2 and Extended Data Fig. 3. D.A.P. obtained and analysed the LT data. A.A.B. led the analysis of the UVOT data. K.L.P. carried out some of the XRT data analysis, particularly the spectral fitting. S.R.O. supported the UVOT data analysis. R.A.J.E.-F. was a co-investigator (Col) of the Chandra observations and was involved in many discussions concerning the interpretation of the object. D.B.M. arranged for the acquisition of the NOT spectrum, helped with its analysis and interpretation, and was a Col for Chandra observations. L.I. conducted the analysis of the NOT spectrum with STARLIGHT. M.R.G. and P.T.O'B. offered AGN expertise that supported the ruling out of AGN activity as the cause of the observed outburst. J.P.O. and B.S. offered programmatic support and general input. All authors read the text and contributed to its editing.

Competing interests

The authors declare no competing interests.

Additional information

Extended data Extended data are available for this paper at <https://doi.org/10.1038/s41550-023-02073-y>.

Supplementary information The online version contains supplementary material available at <https://doi.org/10.1038/s41550-023-02073-y>.

Correspondence and requests for materials should be addressed to P. A. Evans.

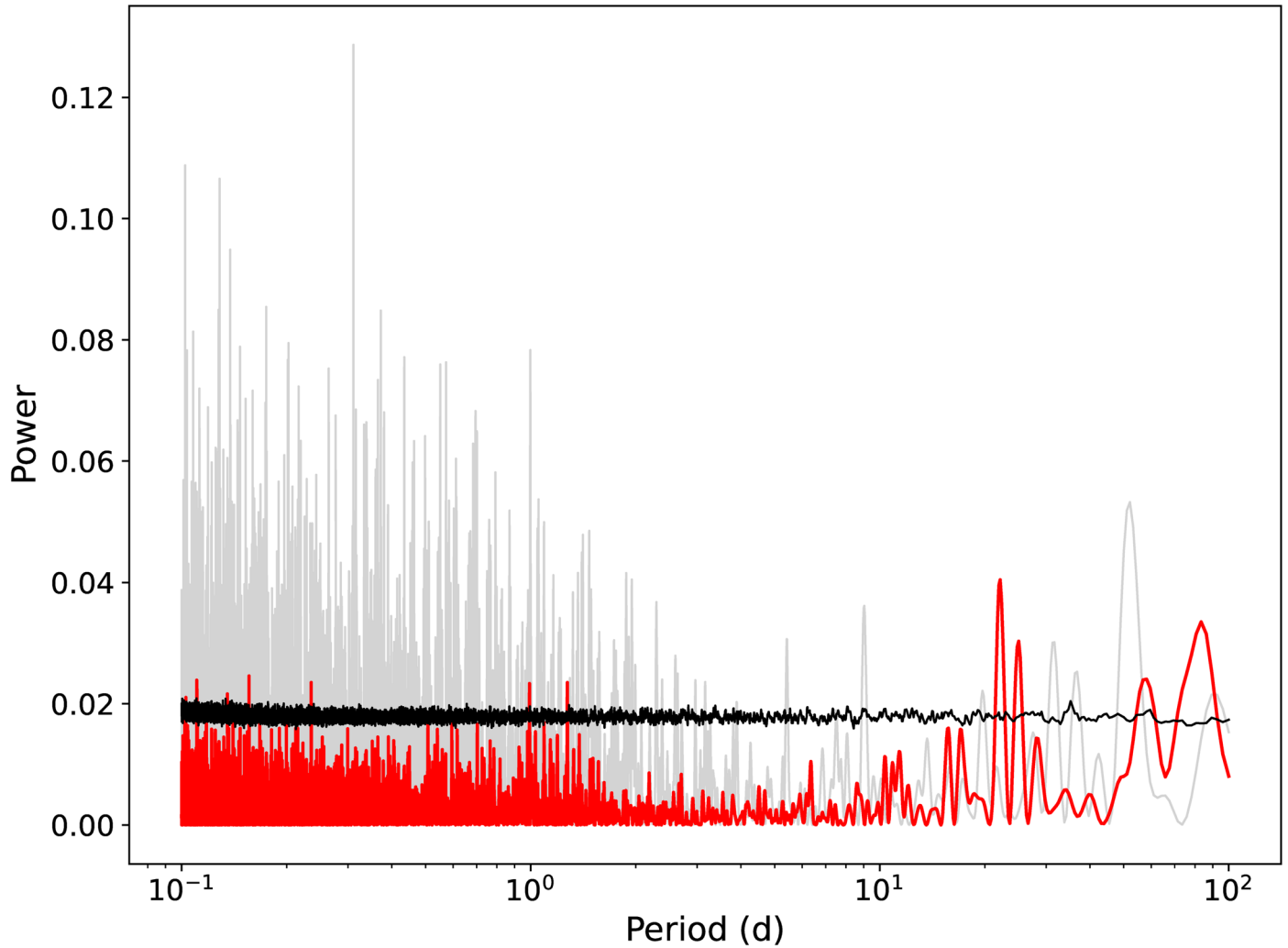
Peer review information *Nature Astronomy* thanks the anonymous reviewers for their contribution to the peer review of this work.

Reprints and permissions information is available at www.nature.com/reprints.

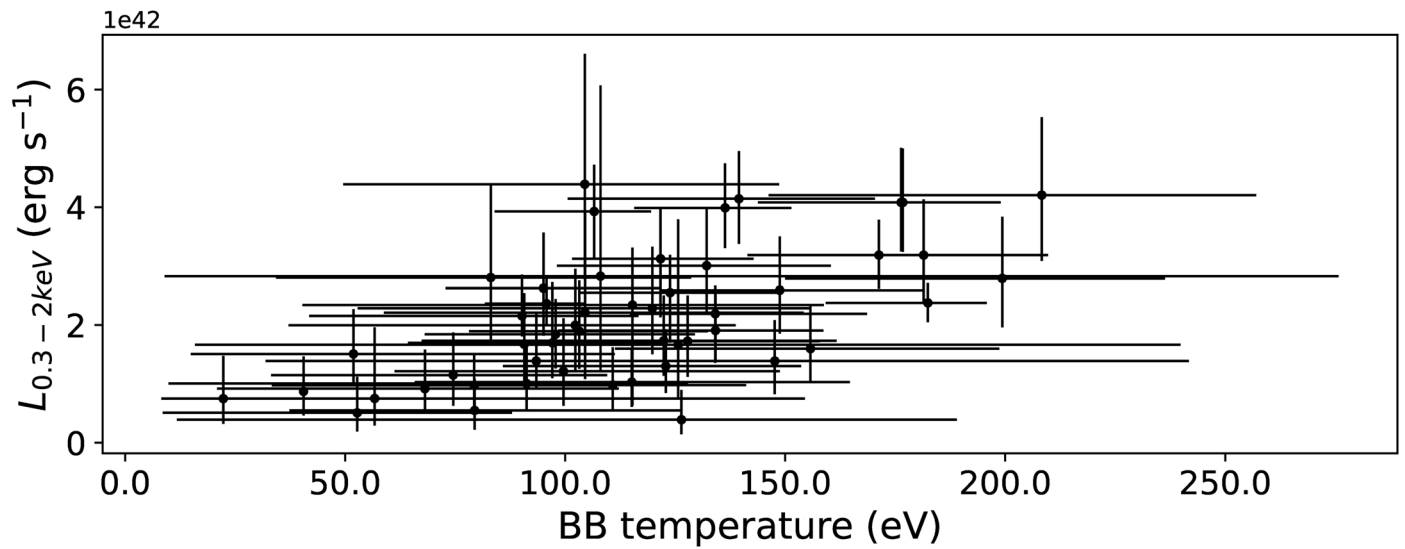
Publisher's note Springer Nature remains neutral with regard to jurisdictional claims in published maps and institutional affiliations.

Open Access This article is licensed under a Creative Commons Attribution 4.0 International License, which permits use, sharing, adaptation, distribution and reproduction in any medium or format, as long as you give appropriate credit to the original author(s) and the source, provide a link to the Creative Commons license, and indicate if changes were made. The images or other third party material in this article are included in the article's Creative Commons license, unless indicated otherwise in a credit line to the material. If material is not included in the article's Creative Commons license and your intended use is not permitted by statutory regulation or exceeds the permitted use, you will need to obtain permission directly from the copyright holder. To view a copy of this license, visit <http://creativecommons.org/licenses/by/4.0/>.

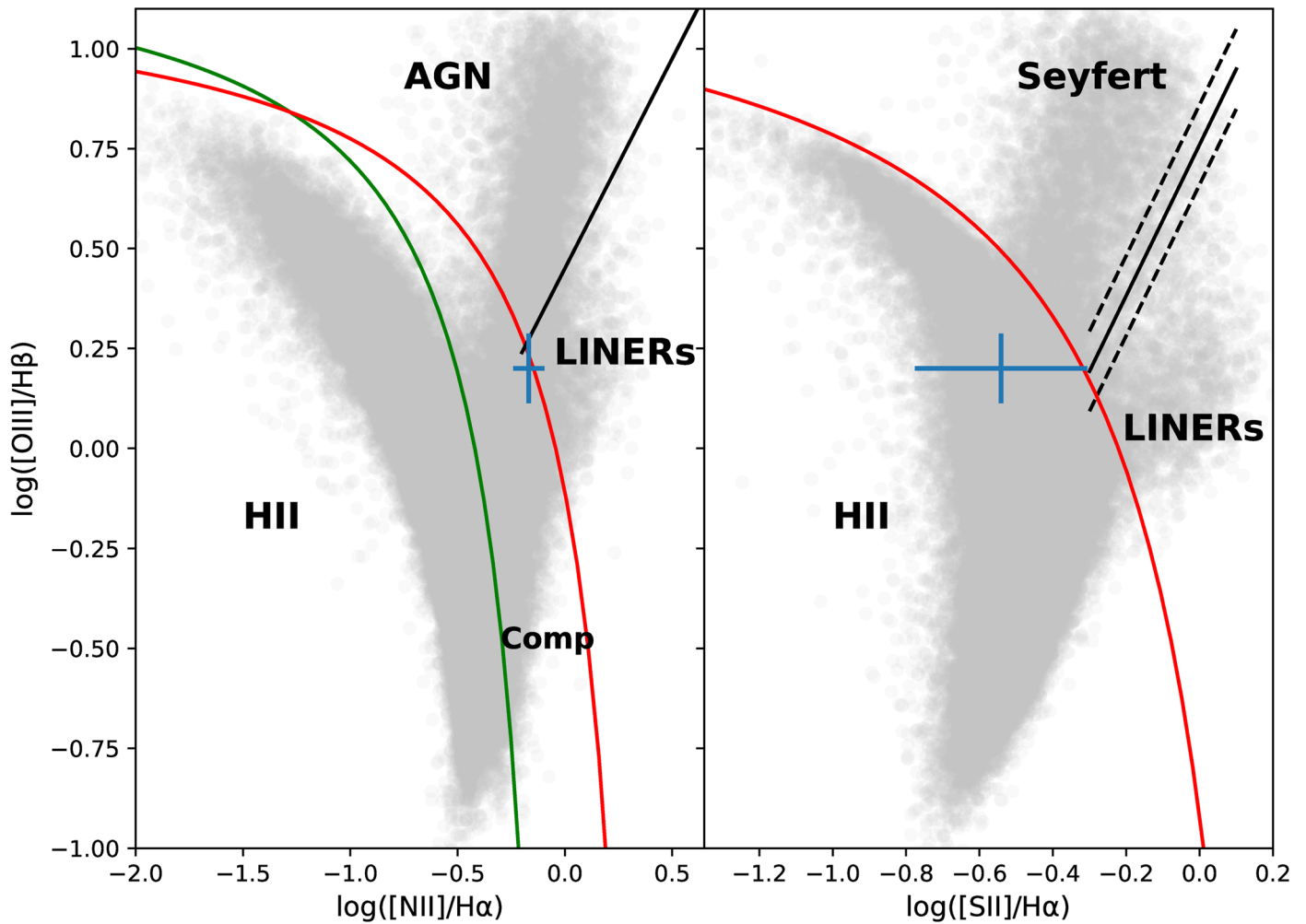
© The Author(s) 2023



Extended Data Fig. 1 | Period analysis of the XRT data of Swift J0230. The Lomb-Scargle periodogram of the per-snapshot binned XRT light curve is shown in red. The window function is in grey and the line marking $3\text{-}\sigma$ significance as a function of period is in black. The two peaks above the $3\text{-}\sigma$ line and not corresponding to window-function peaks are centred on 22.1 d and 25.0 d.



Extended Data Fig. 2 | The 0.3-2 keV luminosity and blackbody temperature derived from spectral fits to the XRT observations in which Swift J0230 was detected. A Spearman rank test shows these to be strongly correlated (p-value: 4.5×10^{-6}). The errorbars reflect the 90% confidence intervals on the parameters, obtained using $\Delta C = 2.706$ in the spectral fitting.



Extended Data Fig. 3 | BPT (Baldwin, Phillips & Terlevich) diagram, showing galaxy type (HII star forming region, AGN, LINER, composite) as a function of certain line flux ratios. The line ratios are $[\text{O III}] 5007 / \text{H}\beta$ versus $[\text{N II}] 6583 / \text{H}\alpha$ (left) and $[\text{S II}] 6717,6732 / \text{H}\alpha$ (right). In both panels, the red solid lines are the theoretical models separating star-forming regions and AGN^{40–43}. In the

left panel, the green line is the demarcation between pure star forming and composite star-forming/AGN regions, as prescribed by. The straight segments separate proper AGN from LINERs. The SDSS galaxy catalogue object density is shown in greyscale and the position of 2MASX J02301709+2836050 is marked by the blue cross (errorbars are 1σ).

Extended Data Table 1 | UVOT photometry from pre-discovery data and the discovery observation

Filter	Magnitude (AB mag)	Magnitude (AB, discovery obs)
v	15.78 ± 0.07	15.82 ± 0.10
b	16.36 ± 0.07	16.41 ± 0.08
u	17.40 ± 0.07	17.41 ± 0.09
uvw1	18.33 ± 0.08	18.39 ± 0.10
uvm2	18.95 ± 0.08	18.88 ± 0.11
uvw2	18.85 ± 0.07	18.91 ± 0.09

Extended Data Table 2 | Liverpool Telescope upper limits on emission at the position of Swift J0230 after subtracting the galaxy emission (AB magnitudes)

MJD-59752	<i>g</i>	<i>r</i>	<i>i</i>	<i>z</i>
7.20	>20.8	>20.8	>20.9	–
32.20	>21.7	>21.6	>21.7	>21.5
25.15	>20.5	>21.2	>21.4	>21.0
29.18	>20.6	>20.7	>20.6	>20.1
33.21	>22.0	>21.2	>19.6	>17.0
66.12	>21.5	>21.6	>21.5	–

I